Chemical Synthesis

Recent progress of *in-situ*/operando characterization approaches of zinc-air batteries

Jian-Feng Xiong[1,2], Meng-Yin Wang[1,2], Ruo-Bei Huang[2,3], Jing-Hua Tian[2,*], Jian-Feng Li[1,2,*] , Zhong-Qun Tian[1,2]

[1]College of Chemistry and Chemical Engineering, Xiamen University, Xiamen 361005, Fujian, China.
[2]Innovation Laboratory for Sciences and Technologies of Energy Materials of Fujian Province (IKKEM), Xiamen 361005, Fujian, China.
[3]College of Materials, Xiamen University, Xiamen 361005, Fujian, China.

Correspondence to: Prof. Jing-Hua Tian, Innovation Laboratory for Sciences and Technologies of Energy Materials of Fujian Province (IKKEM), No. 4221, Xiang'an South Road, Xiang'an District, Xiamen 361005, Fujian, China. E-mail: jhtian@xmu.edu.cn; Prof. Jian-Feng Li, College of Chemistry and Chemical Engineering, Xiamen University, No. 422, Siming South Road, Xiamen 361005, Fujian, China. E-mail: Li@xmu.edu.cn

Abstract

Zinc-air batteries (ZABs) belong to the category of metal-air batteries, with high theoretical energy density, safety, and low cost. Nevertheless, there are still many challenges that need to be solved for the practical application of ZABs, including high overpotential, poor cycle life, and so on. This article first briefly introduced the principle of ZABs, covering the key components, functions of each element, and challenges faced by the system. Subsequently, seven methods for studying ZABs *in-situ* or operando were introduced, including X-ray computed tomography (XCT), optical microscopy imaging (OMI), transmission electron microscopy (TEM), nuclear magnetic resonance imaging (MRI), X-ray diffraction (XRD), Raman spectroscopy, and X-ray absorption spectroscopy (XAS), accompanied by specific research examples. The future perspectives of ZAB characterization have also been discussed.

Keywords: *In-situ* characterization, operando characterization, imaging techniques, spectroscopy techniques, zinc-air battery

INTRODUCTION

The continuous development of the electronics industry, such as electric vehicles, has put forward higher requirements for batteries. Despite gaining widespread attention and application due to their advantages of high output voltage, high discharge power, and long cycle life, traditional lithium-ion batteries have gradually encountered capacity bottlenecks and safety issues during their rapid evolution[1]. It is generally believed that the highest energy density of lithium-ion batteries for practical applications is about 400 Wh·kg^{-1}, while their energy density for current commercial applications is close to this value[2]. In addition, these batteries face problems such as thermal runaway and scarcity of lithium and cobalt resources[3]. Therefore, there is a need to develop a high-energy-density, safe, and resource-rich alternative to lithium-ion batteries.

Inspired by fuel cells, metal-air batteries have attracted extensive attention from researchers. Their negative electrode is metal [including lithium, potassium, sodium, magnesium, aluminum, zinc (Zn), and iron], and the positive electrode is air (the active substance is oxygen) and catalysts. Since the positive active substance is derived from air, there is no need to store the positive reactant in the battery, so the metal-air battery has a very high theoretical energy density [Figure 1][3-5].

Among the various metals, the metal zinc has moderate activity. The advantages of zinc-air batteries (ZABs) include: (1) The possibility of using non-flammable aqueous electrolytes; (2) Mild side reactions in aqueous solution compared to magnesium- and aluminum-air batteries; (3) Relatively high energy density[5]. Thus, ZABs are expected to be promising alternatives to the currently widely used lithium-ion batteries.

Currently, non-rechargeable ZABs have been commercialized and used to power hearing aids because of their small size and large capacity. However, in order to commercialize rechargeable ZABs, there are still some problems that need to be solved, such as short cycle life and high overpotential. The former is caused by variations in the charging and discharging process of the electrode, and the latter arises from the slow cathodic reaction kinetics[6]. These issues can be addressed by studying the battery behavior to achieve insights into the reaction mechanism[7,8].

As we all know, non-*in situ* detection requires disassembling the battery after the charge/discharge is finished. In such cases, only the results of the chemical process can be detected, and no information about the reaction process can be obtained. In contrast, *in-situ*/operando detection is non-destructive or can yield more accurate real-time information, reflecting the reaction process more realistically[9-11].

This paper briefly introduces the composition of ZABs and their associated challenges and then focuses on the application of *in-situ*/operando techniques in their study. Finally, an outlook of *in-situ*/operando characterization for these batteries is given.

STRUCTURES OF ZINC-AIR BATTERIES

The structures of two typical ZABs are shown in Figure 2. Both of them consist of four basic components: zinc metal, air electrodes loaded with bifunctional catalysts, electrolytes, and separators. The common ZABs use an aqueous KOH solution. When discharging, zinc is oxidized to zincate ions at the negative electrode [Equation (1)][12]. At the positive electrode, oxygen passes through the gas diffusion layer and is reduced to hydroxide in the presence of catalysts [Equation (2)]. As the reaction proceeds, zincate in the solution becomes saturated, and zinc oxide precipitates out [Equation (3)]. Since then, zinc can be directly oxidized to form zinc oxide [Equation (4)]. The overall reaction of ZABs [Equation (5)] is that zinc reacts with oxygen to produce zinc oxide.
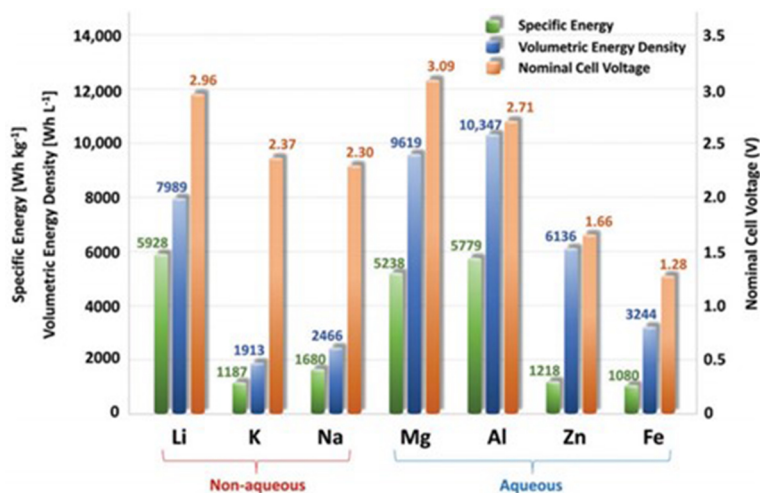
Figure 1. Theoretical specific energy, volumetric energy density, and theoretical battery voltage of metal-air batteries[5].
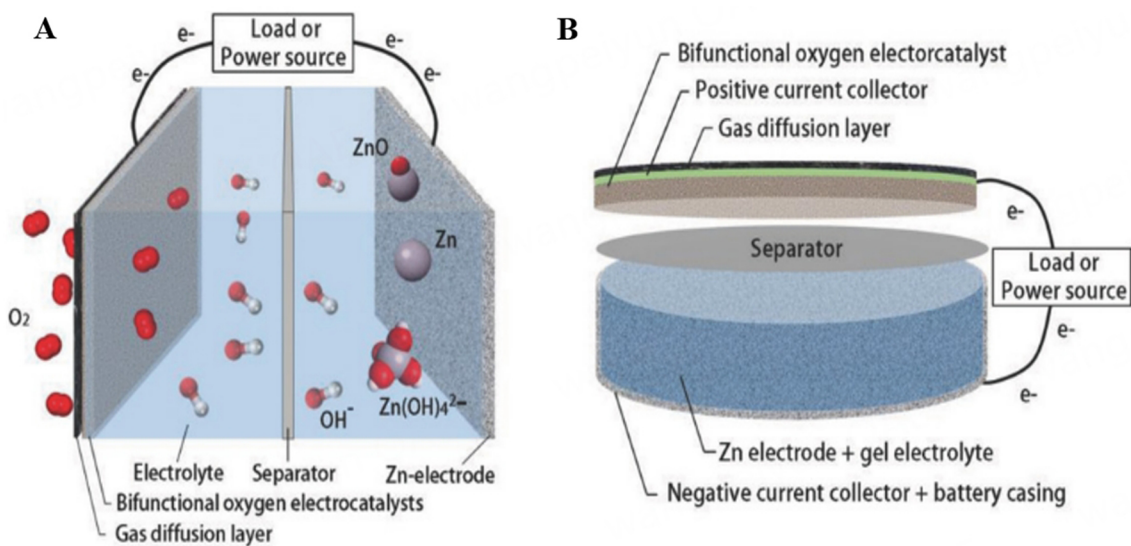
Figure 2. (A) Plate zinc-air battery; (B) Coin zinc-air battery[12].

$$Zn + 4OH^- \rightarrow Zn(OH)_4^{2-} + 2e^- \quad E = \text{-1.26 V } vs.\text{ SHE} \tag{1}$$

$$O_2 + 2H_2O + 4e^- \rightarrow 4OH^- \quad E = 0.4 \text{ V } vs.\text{ SHE} \tag{2}$$

$$Zn(OH)_4^{2-} \rightarrow ZnO + H_2O + 2OH^- \tag{3}$$

$$Zn + 2OH^- \rightarrow ZnO + H_2O + 2e^- \tag{4}$$

$$Zn + O_2 \rightarrow ZnO \quad E = 1.66 \text{ V } vs.\text{ SHE} \tag{5}$$

When the battery is charging, the reverse reaction of the above process occurs.

Zinc anode

The negative electrode form of ZABs is a zinc plate[13] or a mixture of zinc and zinc oxide powder[14]. During charging and discharging, there are several problems with zinc negative electrodes: dendrite formation, shape change, and passivation[5].

Dendrites: During the charging of ZABs, metallic zinc is deposited at the negative electrode:

$$Zn(OH)_4^{2-} + 2e^- \rightarrow Zn + 4OH^- \tag{6}$$

The inhomogeneous negative electrode surface affects the electric field distribution in the solution and the diffusion of zincate[15]. Therefore, different locations on the negative electrode surface have different zinc deposition rates, and inhomogeneous zinc deposition results in the formation of dendrites [Figure 3][16]. In addition, the morphology of the deposited zinc is also affected by the charging current density of the battery and the additives in the solution[17]. The growth of dendrites will cause four problems: large dendrites may break under gravity, disconnect from the electrodes, and cease to participate in charging and discharging. Dendrites can puncture through a separator and contact the positive electrode, causing a short circuit in the battery. They cover the surface of the electrode and hinder the diffusion of zinc-containing ions, affecting the reversible deposition of zinc. Additionally, their generation changes the area of the Zn electrode, affecting the battery power density.

Shape change: Shape change refers to the inability of zinc metal to fully recover on charging after it has changed to zinc salt during discharge. Similar to dendrites, shape change causes a Zn electrode to transform into a fragile and loose shape after repeated charging and discharging, which, in turn, causes some of the electrode material to break away from the electrode[18].

Passivation: Zinc is oxidized directly to zinc oxide [Equation (4)] at high discharge currents that result in a local OH⁻ consumption rate at the negative electrode, which is faster than the rate of diffusion of OH⁻ from the positive electrode to the negative electrode.

Since the oxidation process is in accordance with the shrinking-core theory described by Levenspiel and Guria[19]. For small metallic zinc, such as spherical or ring-shaped [Figure 4A and B], the external zinc oxidizes to zinc oxide and encapsulates the internal zinc [Figure 4C and D], which increases the internal resistance of the battery and prevents the internal zinc from continuing to react, reducing zinc utilization.

The addition of additives or the development of three-dimensional (3D) electrodes can enhance the charge/discharge cycle stability of zinc anodes. For example, adding metals, such as Al, to form an alloy can enhance the crystallinity and improve the cycling performance[20]. Addition of a leveling agent, which adsorbs on the electrode surface to change the electrode/electrolyte interface properties to improve zinc deposition[21]. Designing a 3D porous architecture to enhance the surface area of the Zn electrode, which decreases the local current density on a 3D Zn architecture electrode, resulting in a low over-potential and slow zinc deposition process[22] or build a functionalized protective layer to inhibit hydrogen evolution side

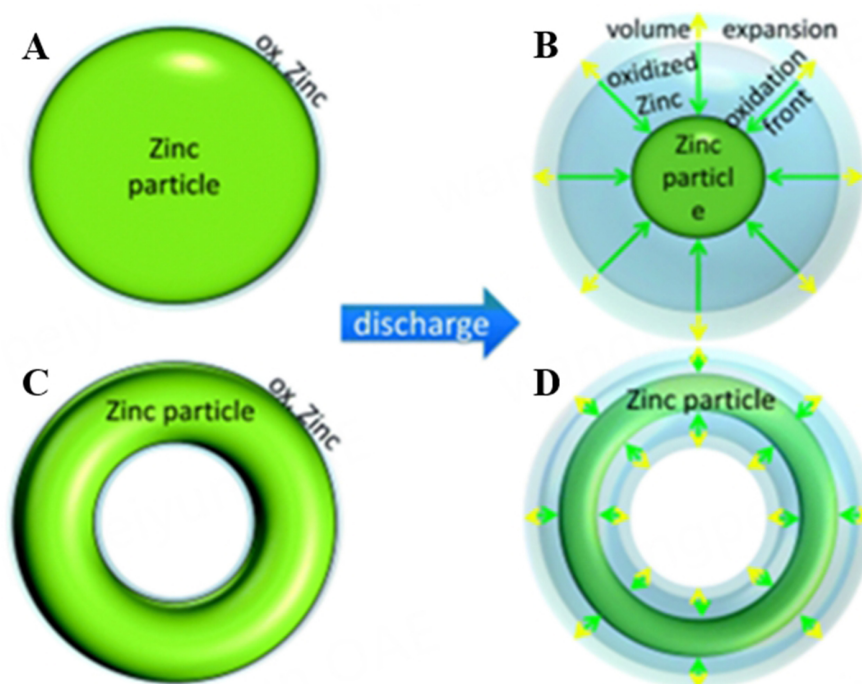**Figure 3.** Dendrites on a zinc electrode[16].

Figure 4. Shrinking-core-concept for zinc oxidation. The oxidation front (green arrows) starts at the particle surface, while volume changes due to the higher density of oxidized zinc are indicated by yellow arrows. (A) Sphere-like zinc particles; (B) Torus-like particles; (C) Sphere-like zinc particles in a partly discharged battery; (D) Torus-like particles in a partly discharged battery[19].

reactions (HER) and surface corrosion[23].

Cathode catalysts

The positive electrode of ZABs is a bifunctional catalyst that catalyzes the reaction with oxygen in the air. Bifunctional means that the catalysts can catalyze both the oxygen reduction reaction (ORR) during discharge and the oxygen evolution reaction (OER) during charging. The excellent catalysts need to have high catalytic activity, be stable to the electrolyte at charge and discharge voltages, and have high selectivity without catalyzing the formation of by-products[6].

According to the material classification, the catalysts commonly used in ZABs are:
(1) Carbon-based catalysts: including N or P-doped graphite[24], N and P-co-doped mesoporous nanocarbon[25], *etc.*

(2) Metal-based catalysts: including metals, metal oxides such as Pt/IrO_2[26] and MnO_2[27], metal sulfides such as Co_9S_8/MnS[28], metal compound catalysts with specific structures, such as perovskite-type oxides: $LaMn_{0.75}Co_{0.25}O_{3-\delta}$, $LaMnO_{3+\delta}$, $PrBa_{0.5}Sr_{0.5}Co_{2-x}Fe_xO_{5+\delta}$, $La_{0.8}Sr_{0.2}Co_{1-x}Mn_xO_3$[29], or layered double hydroxides (LDH) such as CoFeRu-LDH[30], *etc.*
(3) Composite of the above two materials: metal and carbon nanotube (CNT) composite Co_9S_8/CNT[31], CoFe/CoFeN nanotubes[32], metal compound load on nanoparticles on N-doped mesoporous carbon[33], metal and reduced graphene oxide (rGO) composite Co_3O_4-NP/N-rGO[34], MOF-based materials such as Fe-MOF[35], single-atom catalysts such as Fe-N-C[36] and Co-N-C[37], *etc.*

Electrolyte

The electrolyte of ZABs is mainly responsible for dissolving and transporting reactants, such as zinc salts and oxygen reduction products. Since ZABs need to obtain oxygen from the air, the electrolyte needs to have the following properties: (1) non-volatile; (2) stable to the components in the air; (3) high ionic conductivity and oxygen solubility.

Because of the simplicity of preparation and high conductivity, the KOH solution is generally used as the electrolyte for ZABs. However, high concentrations of alkaline solutions are volatile and can deteriorate due to the absorption of CO_2[38]. Besides, the KOH solution experiences HER. As shown in Figure 5, the hydrogen evolution potential of water is higher than the deposition potential of Zn at any pH without considering the overpotential. Obviously, theoretically, the reduction of water to H_2 occurs on charging ZABs ($2H_2O + 2e^- \rightarrow 2OH^- + H_2$ or $Zn+H_2O \rightarrow ZnO + H_2$). In practice, HER is relatively mild due to the presence of overpotential. This reaction can lead to low coulombic efficiency, and the resulting H_2 bubbles can also dislodge dendrites and reduce battery capacity[15].

Electrolyte properties can be improved by adding additives or developing new electrolytes. For example, Adding triethanolamine (TEA), which forms a weak complex with zincate ions that will reduce the solubility of zinc oxide in the electrolyte, can alleviate the deformation problem[39]. The addition of 2% sodium dodecyl benzene sulfonate (SDBS) in a 20% KOH solution can effectively depress the passivation of zinc surfaces during the electrochemical dissolution of zinc and, therefore, improve the discharge capacity of zinc anodes[40]. In addition to this, other types of electrolytes can be used as alternatives, such as neutral solutions[41,42], room-temperature ionic liquids[43], or solid electrolytes[44,45]. However, there may be different reaction mechanisms in different electrolyte solutions[38,46].

Separator

The main function of the separator (or membrane) is to prevent direct contact between the positive and negative electrodes, thereby averting a short circuit[47]. In addition, the separator also (1) Increases the water retention of the battery, slowing down the volatilization of the electrolyte; (2) Prevents zincate ions from migrating to the positive electrode to avoid zincate precipitation caused by positive electrode hydroxide depletion during charging; (3) Restricts the growth of dendrite. An ideal separator should prevent the passage of zincate ions, allow the passage of hydroxide ions, have good mechanical properties, have a wide electrochemical window, and be resistant to alkali[12].

Currently, most studies have focused on the complexes of separators and electrolytes. Most of them are used in flexible or all-solid ZABs[48]. For example, Lee *et al.* reported an electrospun nanofiber mat-reinforced permselective composite membranes[49]. They impregnated polyvinyl alcohol (PVA) into electrospun polyetherimide (PEI) nanofiber mats, and the two acted as ionic size-selective and increased mechanical strength, respectively. Liu *et al.* reported a polydopamine (PDA)-functionalized polyvinylidene fluoride (PVDF) nanofibrous membrane, where the functional groups in PDA (-OH and -NH) promoted the
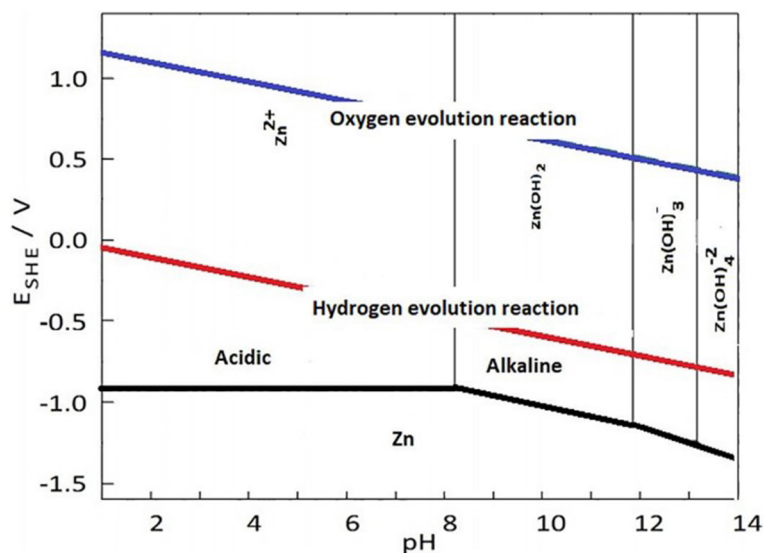
Figure 5. Pourbaix diagram for zinc corresponding to different pH values in water[15].

formation of Zn-O and Zn-N coordination bonds by Zn ions, which resulted in a uniform Zn ion flux for dendrite-free deposition of Zn[50].

According to the composition and structure, battery separators can be generally divided into four types: (1) microporous separators; (2) nonwoven mat separators; (3) polymer electrolyte membrane separators; and (4) composite membrane separators[51]. Their appearance is shown in Figure 6.

*IN-SITU /*OPERANDO CHARACTERIZATION OF ZINC-AIR BATTERIES

In-situ and operando are two different statuses for battery characterization. *In-situ* means in the original position without disassembling and separating. *In-situ* studies are detected without disassembling batteries by designing special device structures. Operando studies detect the chemical process in progress, focusing on time resolution[52].

In-situ/operando detection techniques for ZABs include:
Imaging: X-ray computed tomography (XCT), optical microscopy imaging (OMI), transmission electron microscopes (TEM), magnetic resonance imaging (MRI).
Spectroscopy and pattern: Raman Spectroscopy, X-ray Diffraction (XRD), X-ray absorption spectroscopy (XAS), *etc.*

Finally, the studies corresponding to each technology are summarized in Table 1.

XCT

XCT is a non-destructive 3D imaging technique. The basic principle is that X-rays are absorbed as they pass through an inhomogeneous sample, and the degree of absorption is in accordance with Langbeer's law [Equation (7)]. I and I_o are the intensity of the light after penetration and the intensity of the light before transmission, respectively, μ^i is the attenuation coefficient of the ith substance, and x^i is the distance of the ith substance that the X-rays have passed through[64].

Table 1. Reported *in-situ*/operando studies for ZABs

Method	Research area	In-situ /operando	Cell type	Main result
XCT	Whole battery	*In-situ*	Home-made tubular battery	Leaving space can reduce zinc morphology changes. Catalyst displacement by gas production[53]
			Commercial 300 mAh PR48 cells	Decreasing the discharge current increased the utilized capacity[54]
	Zinc anode	Operando	Home-made tubular battery	Dendrites grow at high current densities and are environmentally controlled[16]
OMI	Zinc anode	Operando	Chip electrochemical cell	Charge current controls zinc deposition, electrolyte affects passivation layer formation[55]
		In-situ	Model battery	Isolated zinc formation leads to reduced battery capacity[56]
			Home-made transparent electrochemical cell	As the current increases, zinc deposition is mainly controlled by thermodynamics, kinetics, and diffusion[17]
TEM	Zinc anode	*In-situ*	Electrochemical liquid cell	In close-packed pure zinc extends in the <10-10> direction[57]
				Lateral growth of zinc dendrites is linearly related to the square root of time when controlled by diffusion[58]
MRI	Electrolyte	*In-situ*	Simulated battery	MRI can observe reactive material convection[59]
Raman spectra	Air cathode	*In-situ*	Simulated battery	Carbon Corrosion Reactions occur: ($C + 6OH^- \rightarrow CO_3^{2-} + 3H_2O + 4e^-$)[60]
XRD	Zinc anode	*In-situ*	Home-made tubular battery	The addition of Bi_2O_3 to the zinc electrode avoids ZnO deposition[61]
				Zn and ZnO conversion initially happens at the top of the anode and progresses downwards over time[14]
XAS	Catalysts	Operando	Simulated battery	Mn^{L+}-N_4 catalysts can be easily poisoned by OH^-. Under applied potential, OH_{ads}-Mn^{H+}-N_4 can be progressively reduced to the Mn^{L+}-N_4 active site[62]
				Se modulators could effectively polarize electron distribution around Cu-N_4 sites and raise their ORR and ZAB activities[63]

MRI: Magnetic resonance imaging; OMI: optical microscopy imaging; ORR: oxygen reduction reaction; TEM: transmission electron microscopes; XAS: X-ray absorption spectroscopy; XCT: X-ray computed tomography; XRD: X-ray diffraction; ZABs: zinc-air batteries.

$$I = I_0 e^{\sum_{i=1}^{n} \mu^i x^i} \tag{7}$$

In a two-dimensional plane, the X-ray source is rotated 360° along the sample, and the transmitted X-ray intensity is detected by a detector. The information of this slice plane can be reduced by Radon transformation. Stacking the slice information gives 3D information in three dimensions.

The advantages and problems of XCT are as follows: Compared to electron microscopy or Raman imaging, XCT introduces more dispersed energy into the system and causes little damage to the sample. It has a higher spatial resolution than optical microscopy and can achieve high contrast with monochromatic X-rays[65]. However, according to its principle, high-contrast images can be obtained by XCT only if the attenuation coefficients between the components within the sample differ significantly. In most cases, a synchrotron light source is required for fast imaging to achieve *in-situ* detection.

Schröder *et al.* designed tube-shaped ZABs suitable for X-ray imaging and used synchrotron XCT to image the battery discharge process[53]. It was shown that the oxidation of zinc caused volume expansion and, thus, pushed the electrolyte into the gas diffusion electrode, isolating the positive electrode from the air and leading to battery failure. Subsequently, Franke-Lang *et al.* further visualized the distribution of zinc particles and produced gases in the cell by optimizing battery structures [Figure 7A][66]. They observed ZnO covering the nuclei of the discharged zinc particles, namely, zinc passivation, and that many gas cavities were produced during discharge. The authors concluded that the loose Zn negative electrode led to separation of the zinc particles from each other during gas generation, increasing the internal resistance of
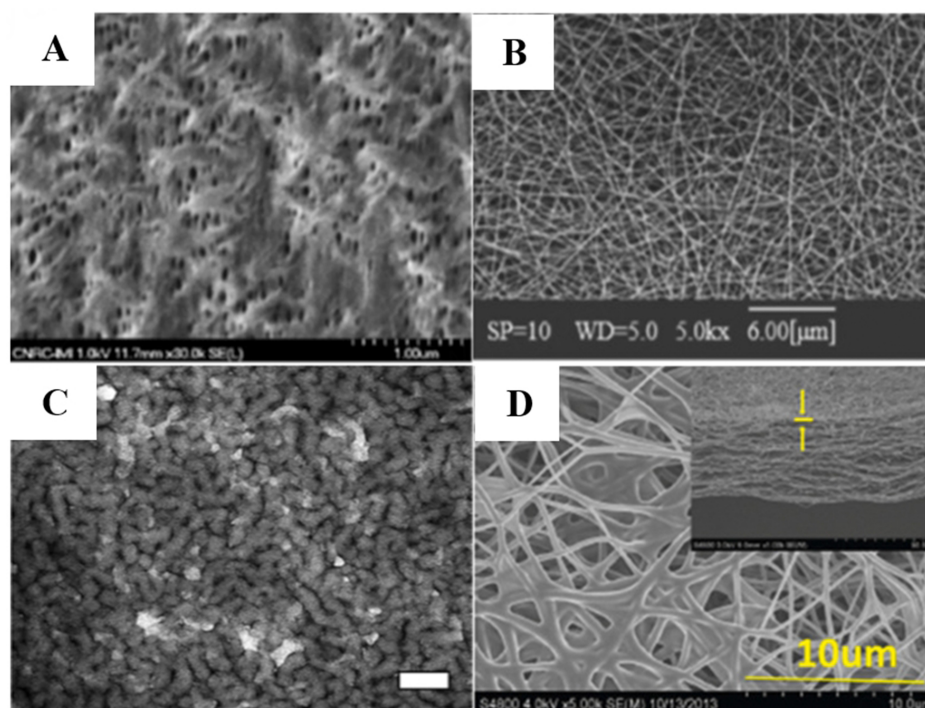
Figure 6. SEM images of (A) Microporous separators; (B) Nonwoven mat separators; (C) Polymer electrolyte membrane separators; (D) Composite membrane separators[51]. SEM: Scanning electron microscopy.

the battery and decreasing the capacity. In addition, the phenomenon that gas generation led to the migration of some zincates to the positive electrode and the gradual deposition of zincates on the positive electrode after several charge/discharge cycles suggests that the structure of the battery needs to be further optimized.

Hack *et al.* used XCT to study the effect of discharge rates on the internal morphology of commercial non-rechargeable ZABs[54]. They found that lowering the discharge current increases the utilized capacity of these batteries. During discharge, Zn close to the separator is preferentially consumed, and the volume reduction of Zn particles deviates from linearity at low current densities. The ZnO particles after discharge are smaller than the Zn particles before discharge, which may be due to the fact that the Zn particles change into multiple ZnO particles during discharge. In addition, as shown in Figure 7B, when the volume-expanded ZnO fills the whole battery, some of the Zn particles in the cell with low discharge multiplicity will leave holes in the original place when they are discharged and disappear.

Yufit *et al.* used synchrotron XCT to study the growth, dissolution, and regeneration of zinc dendrites and the dynamics of zinc dendrite penetration through microporous hydrophilic polypropylene separators under working conditions[16]. It was demonstrated that dendrites preferentially form on inhomogeneous surfaces with highly localized currents. They do not necessarily grow linearly with time as influenced by neighboring dendrites and local currents. Dendrite dissolution starts from the apical dendrite, gradually thinning and breaking off. Finally, it detaches from the electrode surface, after which the electrode body starts to dissolve. When charging again, dendrites still start to grow from the unevenness of the electrode surface and then gradually reattach to the broken dendrites of the previous cycle. The zinc anode will continue to accumulate dendrites after charging and discharging cycles and will not return to the initial dense state. As depicted in Figure 7C, with a separator, the dendrites still grow inside the separator and
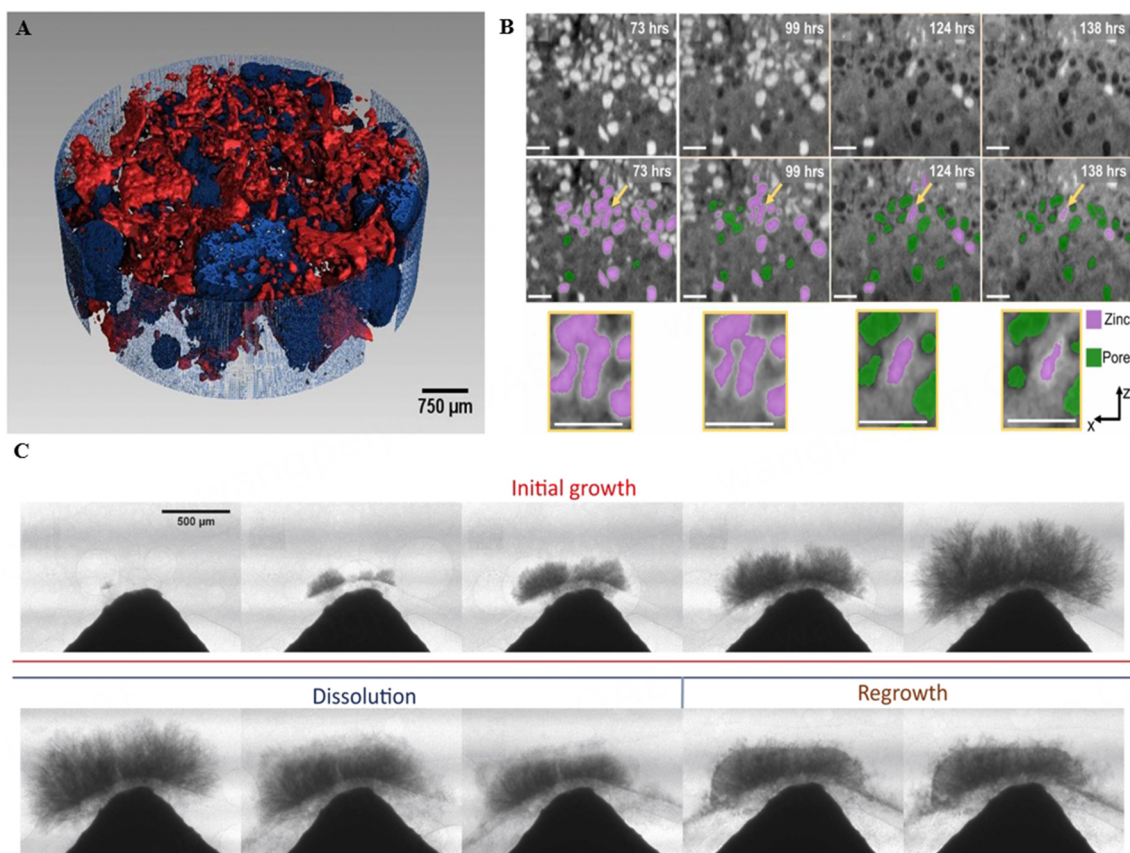
Figure 7. (A) X-ray tomography. Blue is gas cavities, and red is zinc[66]; (B) Zinc particles (red) transform into pores (green) with increasing time[54]; (C) Dendrite growth, dissolution, and regeneration of Zinc-air batteries with porous separators[16].

eventually penetrate it. The presence of a separator significantly affects the growth and morphology of the dendrites, possibly due to mass transfer or current densities, and the dendrites growing inside the separator are denser and more tortuous.

OMI

OMI is the simplest and least expensive means of observation. Its advantages include a simple device, easy implementation, and virtually non-destructive capabilities. Nevertheless, the optical microscope has its drawbacks. For example, it is limited in observing the inner parts of opaque samples, relying on the reflection of light on the surface of the sample or refraction in translucent samples. Additionally, the resolution of optical microscopy is low due to the limitation of visible light wavelength. Despite these limitations, optical microscopy can be used to observe the evolution of morphology and structures, including phenomena such as dendrite growth, volume expansion, and stress[67].

Li *et al.* used a nanohole specular reflection electrode to improve the imaging resolution of optical microscopy and applied it to observe the growth of Zn dendrites in neutral aqueous electrolytes[55]. The method involves etching a nanohole on a substrate and plating a smooth Pt film electrode on the surface of the hole. The Pt electrode undergoes specular reflection, and the Zn on the electrode undergoes diffuse reflection, which can effectively reflect the evolution of Zn dendrites through the difference of the light and dark contrast. As demonstrated in Figure 8A, the authors compared the growth of Zn dendrites in three electrolytes: $ZnSO_4$, $ZnSO_4$ + PEI, and $Zn(OTF)_2$. It was found that in 1 M $ZnSO_4$, the deposition behavior
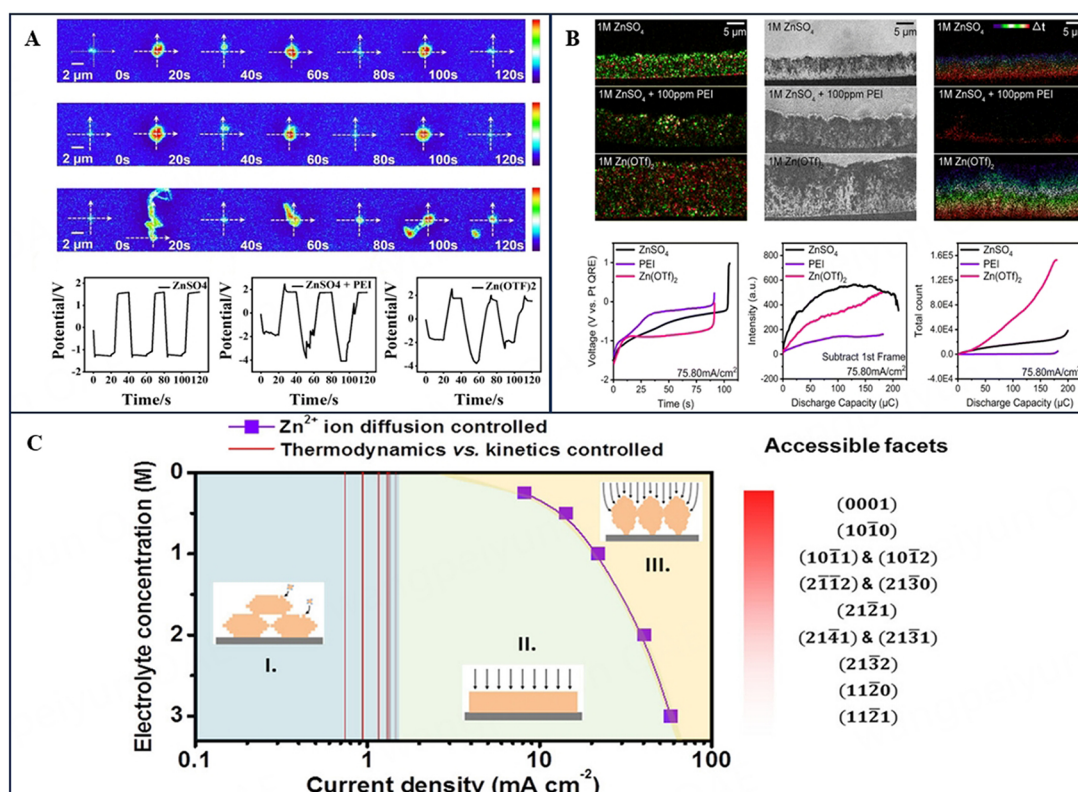
Figure 8. (A) Operando optical observation of the morphology and microstructure evolution of single zinc dendrites during three plating and stripping cycles[55]; (B) Super-resolution analysis and statistics of isolated zinc formation at different charging/discharging current densities[56]; (C) Main factors controlling metal zinc deposition at different current densities[17].

of zinc metal on the nanopore electrode shifted from isotropic to anisotropic with an increasing current, while the growth direction shifted from random to highly oriented. In 1 M $Zn(OTF)_2$, it exhibited a significant dendritic growth pattern, and in 1 M $ZnSO_4$ + ~100 ppm PEI demonstrated the best performance in inhibiting dendrites.

Mao *et al.* used total internal reflection dark-field optical imaging in a neutral electrolyte to study the relationship between charge and discharge rates and the amount and size of Zn detached from the electrode[56]. As shown in Figure 8B, dark-field imaging of the evanescent wave region was performed under two charging/discharging current densities (38 and 189 mA·cm⁻², respectively, denoted as S (slow) and F (fast). It was shown that after charging at high current densities, less isolated Zn and lower overpotentials were generated during discharge at low current densities, resulting in high overall coulombic efficiency. The study also compares the generation of isolated zinc after charging and discharging in three electrolytes: $ZnSO_4$, $ZnSO_4$ + PEI, and $Zn(OTF)_2$. It analyzes the possible reasons for the differences in isolated zinc in different electrolytes.

Cai *et al.* studied the ultrafast zinc metal electrodeposition reaction using OMI[17]. Zinc metal deposition was compared at different current densities and $ZnSO_4$ electrolyte concentrations. It was found that at low current densities, zinc metal tends to be deposited along the (0001) surface with the lowest surface energy; i.e., the reaction process is thermodynamically controlled. In contrast, at medium current densities, the higher-exponential facets with higher surface energies were also activated, and the metal could be deposited in all directions under kinetic control. Then, at high current densities, zinc metal deposition is mainly

controlled by ion diffusion and, thus, has another deposition pattern. The main factors controlling metal zinc deposition at different current densities are shown in Figure 8.

TEM

The TEM uses high-energy electrons instead of visible light for imaging. Thus, its advantage is that it can achieve a resolution of 0.1 nm due to the shorter wavelength of high-energy electrons. However, obtaining such high resolution comes at the cost of harsh usage conditions. For example, the sample needs to be in a vacuum environment, and it must be thin enough for the electron beam to penetrate, usually only about 100~200 nm. Additionally, the sample should be strong and stable enough to withstand the passing electron beam without sustaining damage.

The basic process of TEM is that an electron gun generates a high-speed electron beam, which is then deflected and accelerated by an electric field, undergoes processing with multiple lenses before and after irradiation of the sample, and finally, the electron signals are captured by a fluorescent screen[68].

TEM is mainly used for imaging observation of sample shape, size, and distribution imaging or studying the morphology changes before and after the reaction, such as catalyst agglomeration[69].

In addition, the TEM can also perform an Energy Dispersive Spectrometer (EDS) to qualitatively or semi-quantitatively determine the distribution of elements in the sample[70].

Sasaki *et al.* observed the process of dendrite formation using *in-situ* transmission electron microscopy[57]. They used microelectromechanical system (MEMS) technology to pattern electrodes on Si substrates and electrochemical reactions in a liquid cell holder. As shown in Figure 9A, it was found that dendrite formation is strongly reflected by the *hcp* crystal structure of zinc metal. Nanosized planar hexagonal precipitates of zinc formed dendrites, as evidenced by crystal structural analysis. These dendrites preferably extend along the <10-10> direction in close-packed pure zinc, similar to the dendrites formed by macro-sized experimental systems[71].

Li *et al.* used *in-situ* electrochemical liquid phase transmission electron microscopy (EC-LPTEM) to study the growth of zinc dendrites in a flow cell of $ZnSO_4$ solutions at different currents and electrolyte flow rates[58]. As shown in Figure 9B, the study observed the overpotential at various stages of zinc dendrite growth. In addition, the variation of dendrite length with time was observed by TEM, and it was found that the dendrite growth was well-conformed to diffusion control at low electrolyte flow rates and low currents. Meanwhile, under high electrolyte flow rates and low current conditions, the dendrite growth was partially controlled by reaction kinetics or activation due to sufficient ion supply.

MRI

MRI: A constant magnetic field is applied in space, and the nucleus of an atom is kept in a certain state of motion in the field. If a radio-frequency (RF) magnetic field is applied at the same time, which excites the atom to jump, the energy released when the atom returns to its original state can be detected after the RF field is turned off. At the same time, the relaxation time required for the atom to return to its initial state is detected. The combination of the two allows for the detection of the atomic species and the environment in which it resides[72].

There are three general considerations for the use of MRI in electrochemical studies: (1) The depth of RF penetration into the conducting surface: in accordance with Equation (8). Where δ is the RF skinning depth,
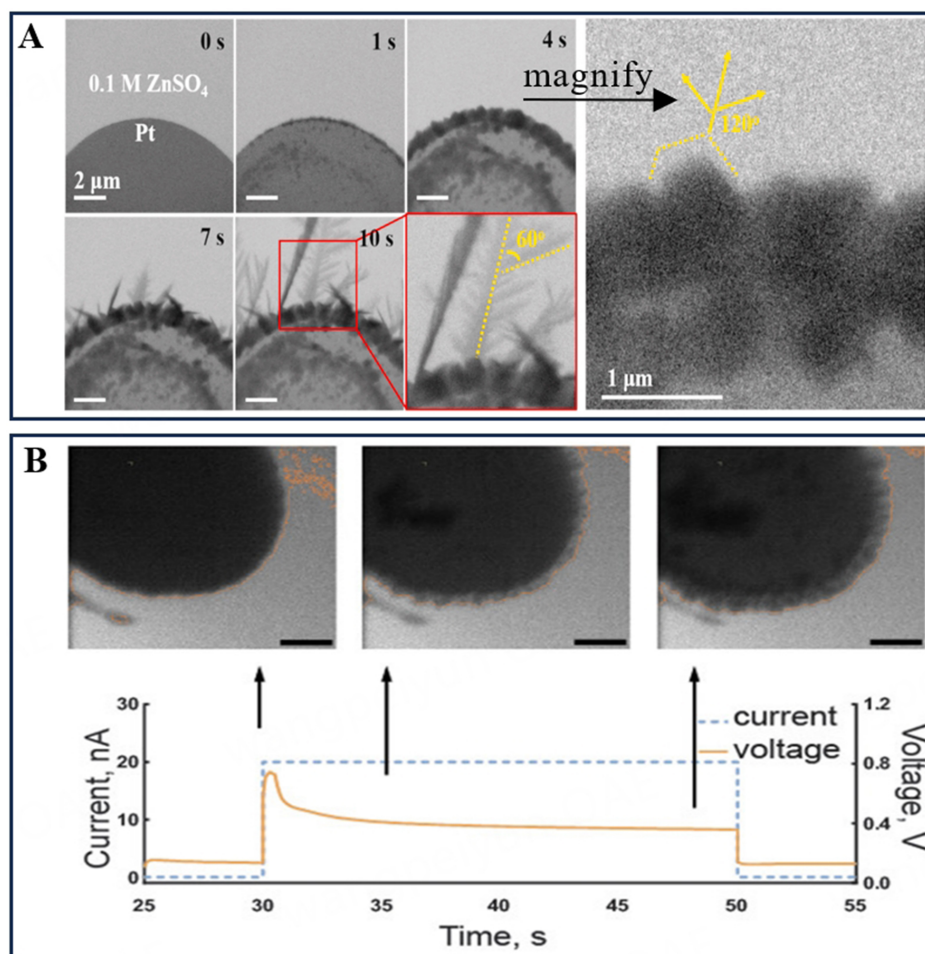
Figure 9. (A) Sequential TEM images of the Zn deposition process on a WE under constant current. The corresponding time from the start of deposition is indicated in each image. An enlarged image at 4 s clearly shows the facets corresponding to the (10-10) planes of hexagonal closed-packed (hcp) Zn metal[57]; (B) A typical Zn electrodeposition process with the corresponding voltage response in the *in-situ* EC-LPTEM test. The scale bar is 2 μm[58]. EC-LPTEM: Electrochemical liquid phase transmission electron microscopy; TEM: transmission electron microscopes. WE: working electrode.

ρ is the resistivity of the conductor, μ_o, μ_r are the vacuum and relative permeability, respectively, and v_o is the Larmor frequency; (2) The RF field passing through the conductor induces eddy currents, which result in a consequent change in the relaxation time of the material within this RF field, producing imaging artifacts; (3) Eddy currents generated at the electrodes directly affect the control of the current of the electrochemical reaction[72].

$$\delta = \sqrt{\frac{\rho}{\pi \mu_0 \mu_r v_0}} \tag{8}$$

Compared to electrode materials, electrolytes, with their high concentrations, narrow linewidths, and relatively long signal lifetimes, are more suitable components for observation using MRI. MRI studies are mainly used to determine the distribution of electrolyte and ion concentrations and measure the mobility of charge carriers. In addition, since the magnetic field penetration is related to the Larmor frequency, the state of the electrode surface can be studied directly or indirectly by adjusting the frequency or studying the distribution of the electrolyte around the electrode.

MRI is a completely non-destructive and fast internal imaging technique. However, its imaging resolution is typically only at the micrometer level, and it can only observe a few specific elements. In addition, MRI has a fatal problem: Metallic conductor materials can interfere with the magnetic field and cause artifacts in MRI imaging.

In 2013, Britton *et al.* reported the use of H MRI to study the changes in the electrolyte during the charging and discharging of ZABs[59]. They were able to minimize metal-induced imaging artifacts by placing a thin sheet of Zn electrodes so that the electrode plane was parallel to the RF magnetic field plane. The artifacts are made to obscure only the surface of the electrode and do not affect the detection of the solution. As shown in Figure 10A, the black shadow on the left side is the Ti electrode sheet, and the black shadow on the right side is the Zn electrode sheet. Because different concentrations of NaOH have varying relaxation times, as displayed in Figure 10B, MRI can image the convection of bases during the reaction. It was found that during the charging and discharging process, there is a certain pattern of convection of the solution around the electrode. The authors attribute this to the directional migration of zincate and hydroxide ions. In addition, the authors noted that because MRI itself induces a magnetic field, imaging creates a potential difference on the Zn sheet. This causes the Zn electrode to discharge at one end and charge at the other, making the measurement results not a good reflection of the real situation.

Raman spectroscopy

Raman spectroscopy involves molecular scattering. When excitation light is shone on a sample, the sample is excited to jump to a certain imaginary state and subsequently emits light of a certain wavelength back to a lower energy state or ground state. The molecule emits light at a wavelength different from the excitation light; i.e., the incident photon may gain or lose energy. This process is known as Raman scattering. Processes such as partial rotation of a molecule, vibrational motion, *etc.*, which cause a change in the polarizability of a molecule, are considered Raman active[73].

The advantages of Raman spectroscopy include its ability to obtain a chemical fingerprint that contains information about the structure of a substance. Raman signals from water are weak, making Raman spectroscopy suitable for detecting aqueous solutions. However, Raman spectroscopy can only provide information about the surface material of the sample. In addition, the ordinary Raman signal intensity is very low; in general, the intensity of Raman scattered light is only one billionth of the intensity of the excitation light. To boost signals, metals, such as gold, silver, copper, *etc.*, can be placed in close proximity to the detected material (a few tens of nanometers). This method is known as Surface Enhanced Raman Scattering[74,75].

Conventional KOH aqueous ZABs do not have substances suitable for detection using Raman spectroscopy. Raman spectroscopy is mainly in some all-solid-state batteries using gel electrolytes or ZABs using ionic liquid electrolytes.

In 2021, Wang *et al.* reported the use of spatially resolved Raman spectroscopy to study the corrosion of the cathode carbon material in alkaline ZABs[60]. Figure 11A shows the Raman spectrum of carbon, while Figure 11B and C shows the spatial distribution of the characteristic Raman peak intensities in Figure 11A. Based on the spatial distribution of the carbonate Raman peaks in Figure 11B, the authors concluded that the carbon electrode is oxidatively corroded to produce carbonate ($C + 6OH^- \rightarrow CO_3^{2-} + 3H_2O + 4e^-$) in an 8 M KOH solution. Meanwhile, the ratio of the intensities of the carbon D and G peaks in Figure 10C shows that the structural disorder of carbon is highest in the region close to the KOH solution, which further proves that the corrosion is a chemical reaction between C and the KOH solution. Eventually, as corrosion
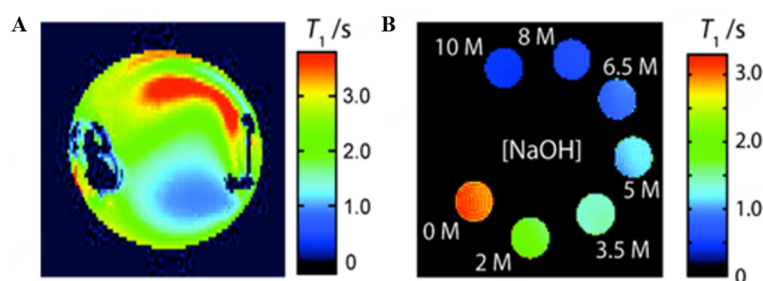
Figure 10. (A) MRI of ZABs; (B) Relaxation time of different concentrations of alkali solutions[59]. MRI: Magnetic resonance imaging; ZABs: zinc-air batteries.
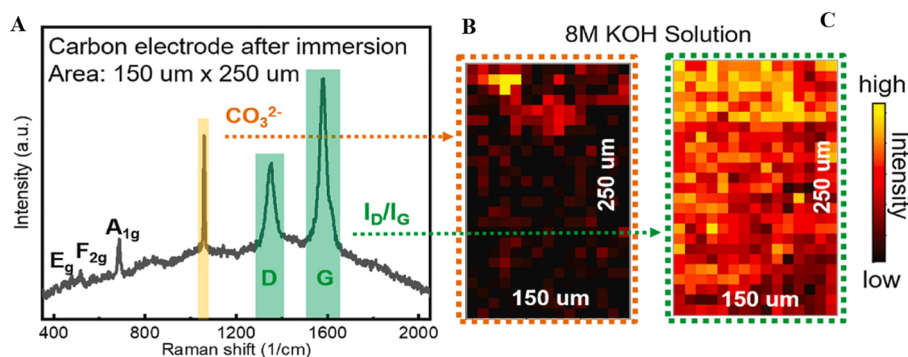

Figure 11. (A) Raman displacement diagram; (B) CO_3^{2-} peak strength at different detection points; (C) Graphite D and G peak intensity ratio I_D/I_G[60].

proceeds, carbonate will precipitate with localized saturation in the porous carbon electrode, which, in turn, affects the battery performance.

XRD

XRD is a technique used to non-destructively characterize crystalline materials. Its advantage is that it allows non-destructive detection of the crystal structure. However, it can only detect ordered crystals and, similar to other X-ray techniques, *in-situ* XRD requires a synchrotron light source to shorten the detection time. In addition, this technique can reflect the mass fraction of each substance in the sample, but this also results in XRD being insensitive to lower content substances[76,77].

XRD is based on the principles that the spacing of periodically arranged atoms in a crystal is of a similar order of magnitude to the wavelength of the X-rays and that X-rays are diffracted as they pass through the crystal, with interference enhancement occurring at a specific angle of diffraction. It probes a sample for overall information, including structural, phase, crystallographic orientation, and average grain size. Additionally, it provides localized information such as crystallinity, strain, and crystal defects[78]. XRD requires a set of diffraction peaks to determine the spatial structure of a substance, and any process that causes a change in crystal structures can be analyzed by it. In ZABs, XRD can be used to study the effects of different electrodes and electrode additives on the dissolution and deposition process of zinc anode. *In-situ* XRD is usually performed during the charging or discharging process of a battery, and XRD maps are collected at different times, which allows the observation of the process of new phase generation, phase transition, or generation of new substances.

In 2018, Santos *et al.* added different masses of Bi_2O_3 to Zn electrodes[61]. They found that with the addition of Bi_2O_3 to Zn electrodes, Bi_2O_3 is reduced by metallic Zn when immersed in KOH electrolytes at an open circuit voltage, with the reaction $Bi_2O_3 + 3Zn + 3H_2O \rightarrow 2Bi + 3Zn^{2+} + 6OH^-$. In addition, it was observed that the addition of Zn electrodes with a 6% Bi mass fraction resulted in enhanced XRD peaks of ZnO due to Zn oxidation during discharge. However, the Zn electrodes with Bi mass fractions of 12% and 25% were not observed to have ZnO peaks, even when fully discharged, as shown in Figure 12A. The authors found that there was no sign of ZnO deposition on the surface of the 12% and 25% electrodes by comparing the scanning electron microscopy (SEM). However, the elemental maps observed the presence of K and Zn on the surface of the electrodes. There may be the presence of $K_2Zn(OH)_4$, and the authors believe that it needs to be confirmed further.

In 2019, Christensen *et al.* used synchrotron XRD and XCT to comparatively study the differences between a single deep charge and discharge and multiple shallow charges and discharges of ZABs and the differences between different positions of the Zn electrodes during charging and discharging[14]. As shown in Figure 12B, during discharge, Zn and ZnO conversion initially happens on the top of the anode, i.e., closest to the cathode, and progresses downwards over time. During charging, the ZnO near the separator is reduced first. After several discharge/charge cycles, the total amount of ZnO did not return to its original value, meaning that it is slowly removed from the anode and migrates to other parts of the battery.

In 2023, Kumar *et al.* found by *in situ* XRD that alkaline electrolytes may form hydroxide species with catalysts, such as $Mo(OH)_2$, on the surface of $NiCoMoO_4$ catalysts, and thus, there may be a spontaneous redox reaction of Zn with Mo species[79].

XAS

XAS or X-ray Absorption Fine Structure (XAFS) determines the absorbance of a material to X-rays of different energies. It utilizes the photoelectric effect of atoms. When an atom absorbs X-rays, the electrons in the atom jump upward from the ground state orbitals[80,81]. For electrons in a certain level, such as those in the orbitals in the M-layer 3d, it would ideally get the jagged absorption peaks, as shown in Figure 13A, such as the M_5-M_1 jagged absorption peak. However, the actual spectrum is shown in Figure 13B, which requires a high resolution (0.1 eV) to be recognized due to the similarity of the energies required for the different group state leaps.

In addition, according to the energy of the X-ray light source, XAS can be divided into Near-Edge X-ray Absorption Fine Structures (XANES) and Extended X-ray Absorption Fine Structures (EXAFS). XANES contains the region from before the absorbing edge to 50 eV after the absorption edge. EXAFS refers to the region from 50 to 1,000 eV behind the absorption edge.

The advantage of XAS is that it is complementary to XRD and can obtain information about the structure of an atom and its surrounding ligands. In the XANES region, the absorption signals are clear and easy to measure. The short acquisition time makes it suitable for time-resolved experiments. It is sensitive to chemical information such as valence, unoccupied electronic states, and charge transfer. Besides, XAS is less affected by temperatures; it can be used for high-temperature *in situ* chemistry experiments and has a simple fingerprinting effect, which can be used to quickly recognize the structure of an object.

The problem with XAS is similar to other X-ray techniques in that its detection quality is greatly affected by the intensity of the light source and the purity of the sample.
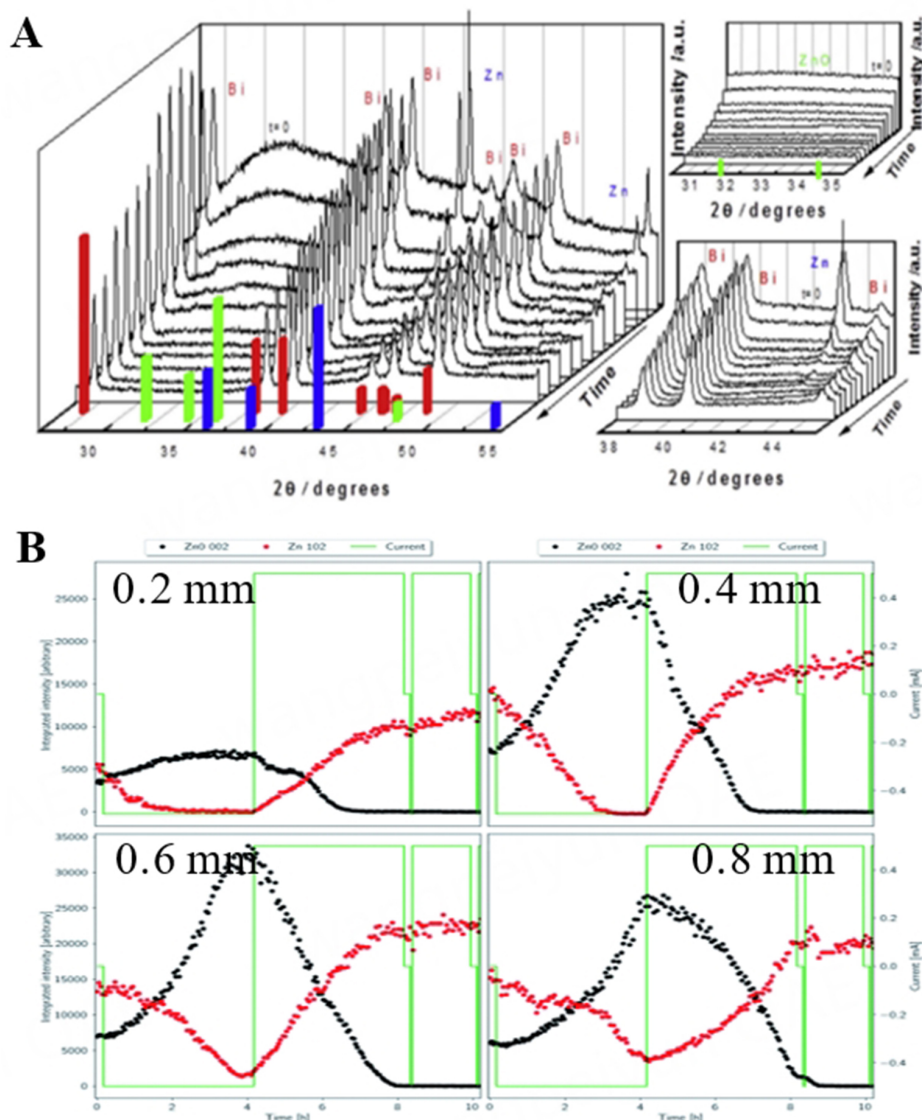
Figure 12. (A) XRD patterns of Zn electrodes containing 25% Bi_2O_3 during discharge[61]; (B) XRD patterns of Zn electrodes during charging and discharging at different positions in the anode starting[14]. XRD: X-ray diffraction.

In situ XAS is commonly used to observe changes in catalyst structures, valence, and coordination information during the reaction process, which can be used to infer the active site of the catalyst, the reaction intermediate species, and, thus, the reaction mechanism[83].

Han *et al.* developed a single-atom site catalyst with a Mn-N_4 structure suitable for ZABs and investigated its dynamic atomic structure for the ORR process in alkaline electrolytes on a working XAS device[62]. It was shown that Mn^{L+}-N_4 is easily poisoned by OH$^-$ in the electrolyte. At the applied potential [Figure 14A and B], a reduction reaction occurs: OH_{ads}-Mn^{H+}-$N_4 \rightarrow Mn^{L+}$-N_4 + OH$^-$, and the reduced Mn is the active site of the reaction. DFT calculations demonstrate that the atomically dispersed Mn^{L+}-N_4 site promotes electron transfer to the *OH species.
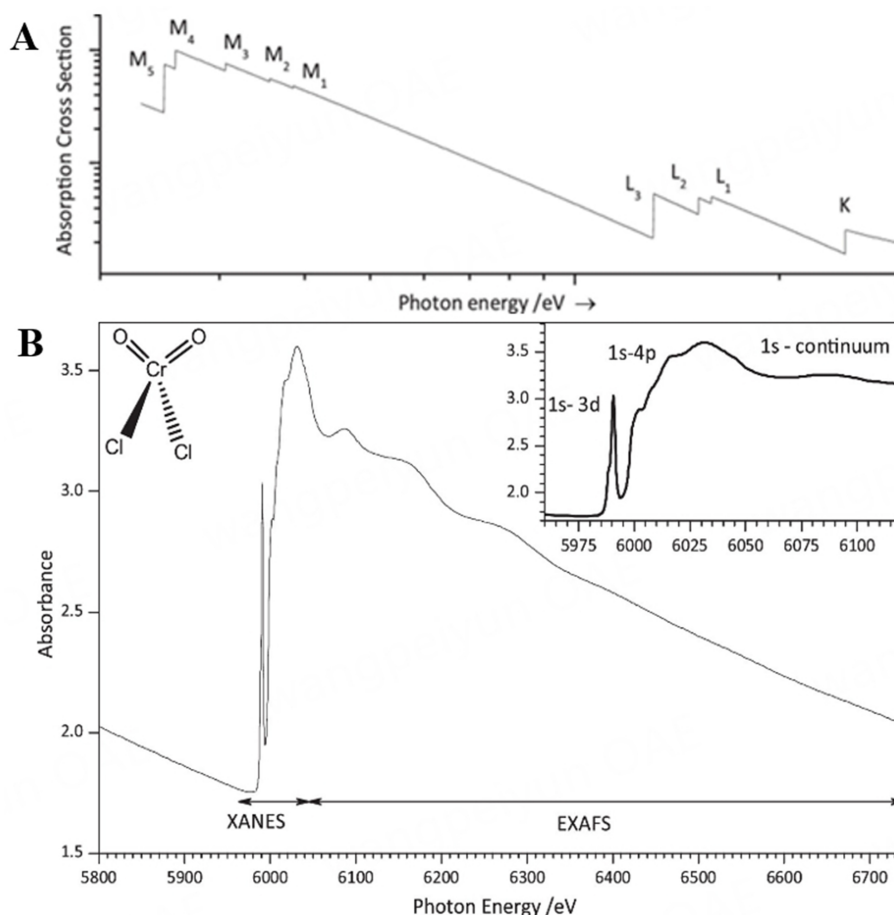
Figure 13. (A) Ideal XAS spectra[82];(B) Cr K-edge XAFS spectrum of CrO_2Cl_2 at 10 K, showing the division of the XAFS spectrum into the XANES and EXAFS regions[82].EXAFS: Extended X-ray Absorption Fine Structures; XANES: Near-Edge X-ray Absorption Fine Structures; XAS: X-ray absorption spectroscopy.

Sun *et al.* developed a diatomic catalyst (Cu-Se DAs) consisting of asymmetric $Cu-N_4$ and $Se-C_3$ active sites[63]. They applied the synthesized catalyst to a ZAB and used work XAS coupled with synchrotron infrared spectroscopy to detect the electronic and atomic evolution of the Cu sites [Figure 14C and D]. The XAS results showed that the catalyst was not damaged by the alkaline electrolyte. As the potential increased from 0.4 to 1.0 V *vs.* Zn, the valence state of Cu slightly increased, the Cu-O coordination number increased from 0.3 to 1.0, and the adsorption of surface intermediate species OOH* was enhanced. It is demonstrated that Se sites can effectively facilitate the transition from $OOH^*-(Cu_1-N_4)$ to subsequent $O^*-(Se_1-C_2)$ intermediates. This atomic-level synergistic catalytic effect can effectively increase the four-electron ORR activity and enhance the catalyst performance.

CELL CONFIGURATIONS OF *IN-SITU* /OPERANDO ZINC-AIR BATTERIES
Tubular battery
Tubular batteries are similar in structures to coin batteries, but tubular batteries have a higher thickness of electrode material per layer, so it is possible to study how the electrode material changes during the reaction at different distances from the separator. Since it cannot be squeezed akin to a coin cell, this device generally relies on springs or threads to compress the cell. This design is primarily used for XRD and XCT measurements. In general, these devices simply use a synchrotron light source to shorten the detection time and enable *in-situ* detection.
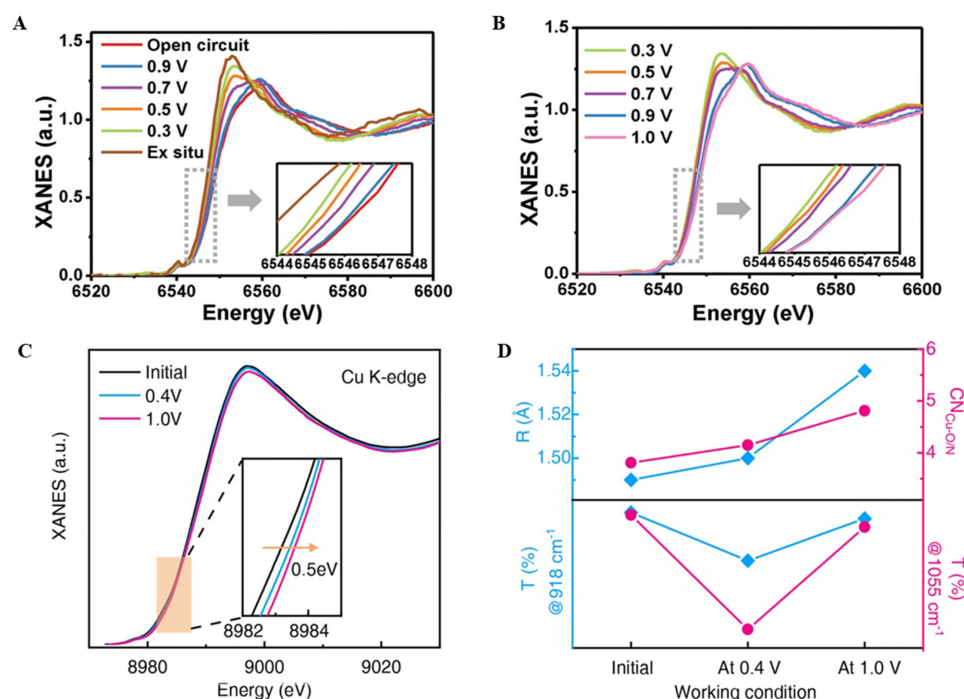
Figure 14. (A) Operando XANES under the open-circuit condition and at potentials ranging from 0.9 to 0.3 V; (B) Operando XANES when the applied potentials were reversed[62]; (C) The operando Cu K-edge XANES spectra at different voltages. The inset shows the magnified adsorption-edge region; (D) The difference in the location of the main peak and the Cu-N/O coordination number and the intensity difference of the infrared signals at 918 and 1,055 cm^{-1} change with applied potentials for Cu-Se DAs during the ORR process[63]. DAs: Diatomic catalyst; ORR: oxygen reduction reaction; XANES: Near-Edge X-ray Absorption Fine Structures.

Franke-Lang *et al.* constructed an *in-situ* XCT device [Figure 15A][66]. The cell is the same size as AAA batteries, and the cell pressure can be adjusted by rotating a fixed plunger. The cell casing material is PTFE, which balances chemical stability and X-ray transmission. The gas diffusion electrode has a gold mesh as a current collector, the Zn electrode has a cylindrical graphite spacer as a current collector, the zinc negative electrode uses paste slurry containing KOH electrolytes, and the gas diffusion electrode uses a mixture of dried and homogeneously dispersed catalyst and conductive carbon.

The *in-situ* XRD setup used by Santos *et al.* is shown in Figure 15B[61]. The most important feature of this cell is that the Zn electrode is pressed against a copper collector with high pressure and attached to a screw used to lift the electrode, which adjusts the thickness of the X-rays through the liquid layer, thus enabling small angle XRD measurements. The Zn electrode side of the cell is sealed with a polypropylene film to prevent electrolyte leakage. Figure 15C shows the *in-situ* tubular battery designed to be suitable for *in-situ* XRD and XCT used by Christensen *et al.*[14]. Two capillary tubes were filled with positive and negative slurry, a separator was added, and one capillary tube was inserted into the other, with two wires drawn as leads.

Simulated battery

Simulated *in-situ* batteries represent simple improvements on three-electrode electrochemical cells. Two electrodes of such *in-situ* batteries are far apart, the interaction is weak, and there is generally no separator. The study focuses on the behavior of one electrode. This type of electrochemical *in-situ* cell generally only requires optimization of the direction of the Raman excitation light/RF magnetic field and its thickness through the liquid layer to irradiate the study area.
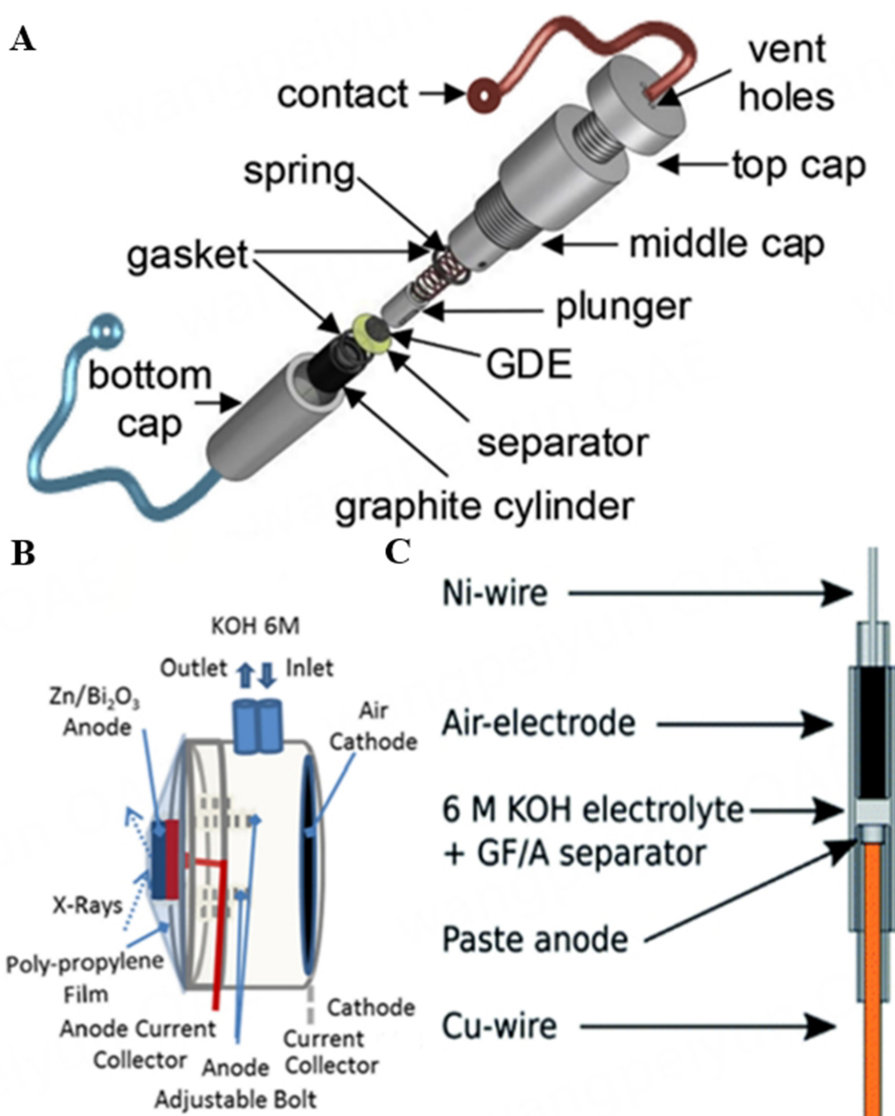
Figure 15. (A) Tubular *in-situ* battery structure[66]; (B) Scheme of the electrochemical cell used in the synchrotron XRD measurements[61]; (C) Schematic illustration of the capillary ZABs[14]. XRD: X-ray diffraction; ZABs: zinc-air batteries.

The *in-situ* simulated battery of ZABs for MRI study was reported by Britton *et al.*[59]. They used Zn and Ti plates as the negative and positive electrodes of the battery, respectively, and 1 M NaOH solution as the electrolyte. Artifacts caused by eddy currents in the metal can be minimized by orienting the static magnetic field direction perpendicular to the metal sheet (X-axis) and the RF magnetic field along the Z-axis. As shown in Figure 16A, MRI can image the H-containing species in the medium to observe the diffusion and convection of the electrolyte.

Wang *et al.* reported the *in-situ* Raman characterization of ZAB cathode catalysts[60]. A three-electrode *in-situ* cell was used for the study, with the working electrode as a carbon electrode and a Pt mesh and Hg/HgO electrode as the counter electrode and reference electrode, respectively. An 8 M KOH solution containing saturated ZnO was used as the electrolyte. As shown in Figure 16B, the working electrode was tightly attached to the Ni mesh collector at the edge of the cell for cross-section observation. Simultaneous sampling using multi-point Raman was also performed to obtain spatially resolved Raman spectra, which,
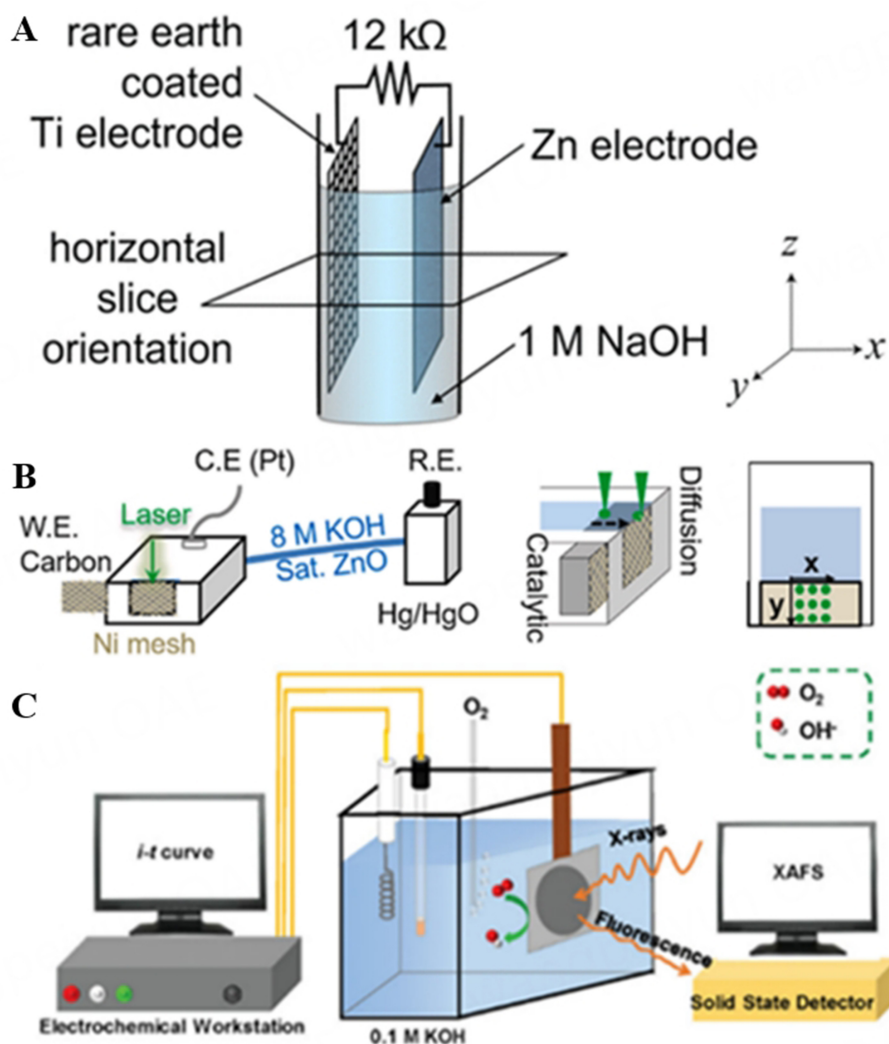
Figure 16. (A) Schematic representation of the full ZAB when under the constant load discharge condition, illustrating the horizontal image orientation. The diameter of the vial is 12 mm[59]; (B) Illustrations of three-electrode system *in-situ* Raman measurements and multi-point Raman mapping apparatus[60]; (C) Experimental setup of an operando XAS device[62]. XAS: X-ray absorption spectroscopy; ZAB: zinc-air batterie.

in turn, investigated the corrosion of carbon electrodes at different locations from the electrolyte.

Similarly, Han *et al.* measured the catalyst of ZABs using a home-made operando XAS cell, and in order to distribute the catalyst throughout the electrode and to make full contact with the electrolyte, porous carbon cloth was used as the working electrode, and the whole test setup of its schematic is shown in Figure 16C[62].

Specially designed *in-situ* batteries
Some *in-situ* batteries generally have special detection principles and, therefore, require corresponding special structural designs.

For example, Mao *et al.* designed an *in-situ* cell based on the principle of total internal reflection dark-field microscopy (TIRDFM)[56]. As shown in Figure 17A, this system illuminates Zn near the electrode interface using fading waves, greatly improving the observation accuracy (~10 nm) through a special optical path
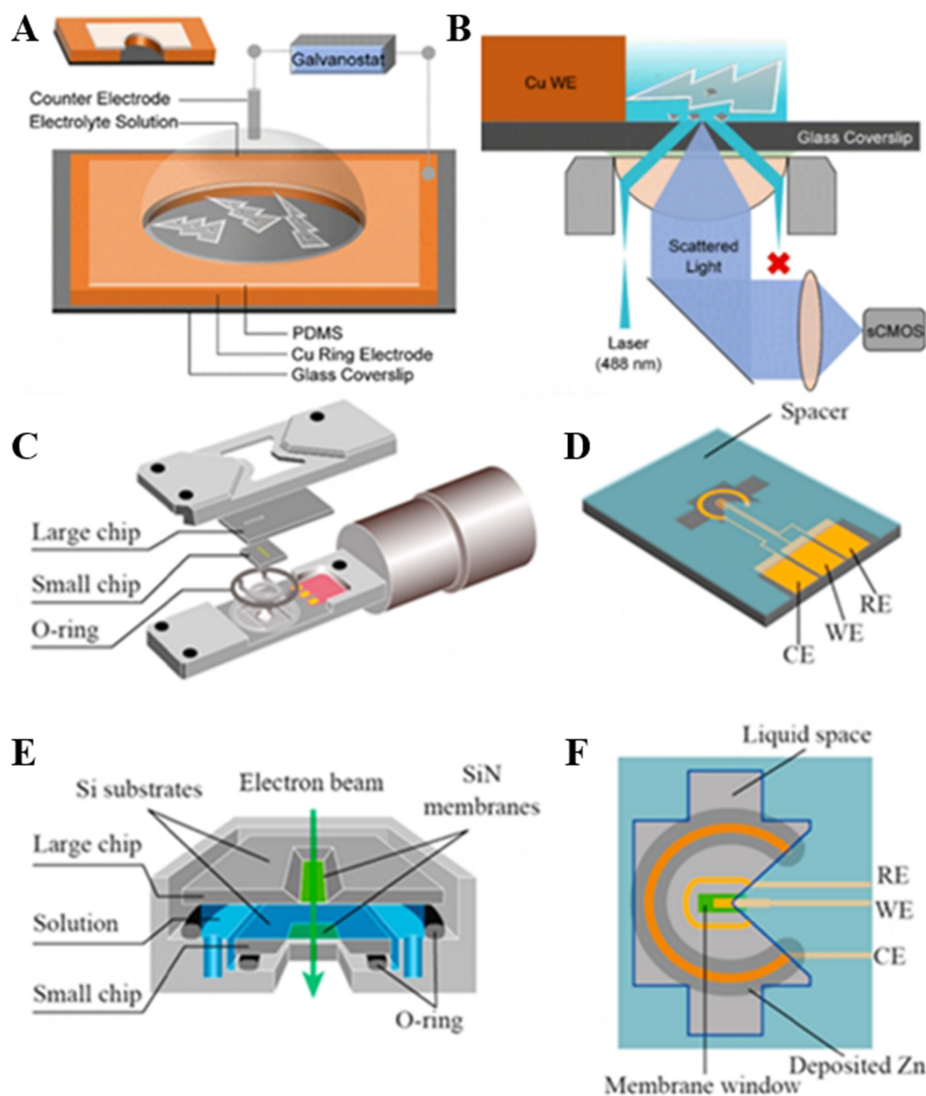
Figure 17. Schematic illustration of the experimental setup. (A) A model zinc-air battery with the cross-section view of the cell in the upper-left corner (electrochemical setup); (B) *In-situ* TIRDFM (reflected light is rejected)-based setup used to collect scattered light during the zinc-plating process[56]; (C) Schematic diagram of a liquid battery holder for observing electrochemical reactions in the solution; (D) Cross-sectional view of the battery; (E) Design drawing of the MEMS chip of the electrodes; (F) Arrangement of the three electrodes on the chip[57]. MEMS: Microelectromechanical system; TIRDFM: total internal reflection dark-field microscopy.

design [Figure 17B] that avoids receiving total internal reflection and specular reflection light. Instead, it only captures the scattered light from the electrode to improve the signal-to-noise ratio. The authors were able to observe the isolated Zn falling off the electrode at the bottom with this system.

Sasaki *et al.* fabricated a miniature three-electrode cell by patterning three Pt electrodes on a Si substrate by using MEMS technology, and the overall structure is shown in Figure 17C and D[57]. The cell consists of two Si substrates with an ultrathin 5 nm silicon nitride film window in the middle of the cell to allow TEM electron beam penetration. The electrolyte of the cell is connected to a syringe pump external to the TEM through a polyether ether ketone (PEEK) tube, which allows the flow of solution by pushing the syringe with a motorized vise. The three electrodes are arranged, as shown in Figure 17E and F, with the electrodes at a constant distance from each other. For use, Zn was first deposited on the counter electrode. The system

meets the high vacuum requirements of the TEM technique by sealing, but the cell body is very thin in order to allow the electron beam to pass through, and the diffusion behavior of the reacting species may be different from that of a real battery.

CONCLUSION AND OUTLOOK

ZABs are low-cost, high-safety, high-energy-density fuel cells with unique advantages in large-scale energy storage. However, the poor performance of cathode catalysts, irreversibility in zinc anode cycling, and electrolyte deterioration limit their industrial application. Additionally, a systematic theoretical model is still lacking to understand the failure mechanism of ZABs in different systems.

In situ/operando characterization can obtain information about the material properties of the system under study at different times and potentials and is a must for a deeper understanding of the reaction process. However, existing *in-situ*/operando devices are rarely able to balance the appropriate reaction conditions and obtain high-quality detection signals. Compared to Li-ion batteries, ZABs require less sealing, and finding cell materials that are stable under their operating conditions facilitates *in-situ*/operando studies. In fact, most of the techniques suitable for ZABs can be realized for *in-situ* detection as long as the conditions are suitable. For example, mass spectrometry-based sampling and detection techniques need to ensure that the sample volume is low enough. Techniques that require a high vacuum can seal the cell with a strong, ultra-thin window. Trace species that cannot be detected due to insufficient signal strength can also be detected using enhanced light sources or surface-enhanced spectroscopy.

We believe that the future design of *in-situ*/operando cells should focus on the following three issues: (1) Ensure that the cell material is chemically stable in strong alkali or electrolytes containing organic additives and that there is no interference with battery operation and detection; (2) Define the area of interest for the study and boost the strength of the received signal. Operando studies also require ensuring the timeliness of the received signals; (3) Construct the device structure to approach the real battery as much as possible.

In addition, the combination of multiple techniques is important. This involves not only combining the aforementioned *in-situ*/operando characterization techniques to obtain complementary information but also amalgamating characterization techniques with time and spatial resolution. Additionally, combining characterization techniques with theoretical calculations is essential for a comprehensive understanding. However, the challenge in combining these techniques lies in the fact that, in most cases, it is difficult to test both techniques at the same time. Consequently, varying testing times may result in batteries being in disparate states, even at the same potential, thus preventing the accurate correlation of results obtained by the two techniques with each other.

We believe that to truly understand ZABs, more emphasis needs to be placed on *in-situ*/operando condition studies in the future.

DECLARATIONS

Authors' contributions
Prepared the manuscript: Xiong JF, Wang MY, Huang RB
Designed and revised the manuscript: Tian JH, Li JF, Tian ZQ

Availability of data and materials
Not applicable.

Conflicts of interest
All authors declared that there are no conflicts of interest.

Ethical approval and consent to participate
Not applicable.

Consent for publication
Not applicable.

REFERENCES

1. Chen Y, Kang Y, Zhao Y, et al. A review of lithium-ion battery safety concerns: the issues, strategies, and testing standards. *J Energy Chem* 2021;59:83-99. DOI
2. Eftekhari A. On the theoretical capacity/energy of lithium batteries and their counterparts. *ACS Sustainable Chem Eng* 2019;7:3684-7. DOI
3. Liu JN, Zhao CX, Wang J, Ren D, Li BQ, Zhang Q. A brief history of zinc-air batteries: 140 years of epic adventures. *Energy Environ Sci* 2022;15:4542-53. DOI
4. Fu J, Liang R, Liu G, et al. Recent progress in electrically rechargeable zinc-air batteries. *Adv Mater* 2019;31:1805230. DOI
5. Fu J, Cano ZP, Park MG, Yu A, Fowler M, Chen Z. Electrically rechargeable zinc-air batteries: progress, challenges, and perspectives. *Adv Mater* 2017;29:1604685. DOI
6. Ren S, Duan X, Liang S, Zhang M, Zheng H. Bifunctional electrocatalysts for Zn-air batteries: recent developments and future perspectives. *J Mater Chem A* 2020;8:6144-82. DOI
7. Zhang D, Hu W. Study on failure mechanism on rechargeable alkaline zinc-air battery during charge/discharge cycles at different depths of discharge. *Front Chem* 2023;11:1121215. DOI
8. Yadav SK, Deckenbach D, Schneider JJ. Secondary zinc-air batteries: a view on rechargeability aspects. *Batteries* 2022;8:244. DOI
9. Li H, Guo S, Zhou H. In-situ/operando characterization techniques in lithium-ion batteries and beyond. *J Energy Chem* 2021;59:191-211. DOI
10. Sun Z, Zhang Y, Liu Y, Hou L, Yuan C. Recent progress on in situ/operando characterization of rechargeable alkali ion batteries. *ChemPlusChem* 2021;86:1487-96. DOI
11. Liu D, Shadike Z, Lin R, et al. Review of recent development of in situ/operando characterization techniques for lithium battery research. *Adv Mater* 2019;31:1806620. DOI
12. Chen X, Zhou Z, Karahan HE, Shao Q, Wei L, Chen Y. Recent advances in materials and design of electrochemically rechargeable zinc-air batteries. *Small* 2018;14:1801929. DOI
13. Yu W, Shang W, He Y, Zhao Z, Ma Y, Tan P. Unraveling the mechanism of non-uniform zinc deposition in rechargeable zinc-based batteries with vertical orientation. *Chem Eng J* 2022;431:134032. DOI
14. Christensen MK, Mathiesen JK, Simonsen SB, Norby P. Transformation and migration in secondary zinc-air batteries studied by *in situ* synchrotron X-ray diffraction and X-ray tomography. *J Mater Chem A* 2019;7:6459-66. DOI
15. Hosseini S, Masoudi Soltani S, Li YY. Current status and technical challenges of electrolytes in zinc-air batteries: an in-depth review. *Chem Eng J* 2021;408:127241. DOI
16. Yufit V, Tariq F, Eastwood DS, et al. *Operando* visualization and multi-scale tomography studies of dendrite formation and dissolution in zinc batteries. *Joule* 2019;3:485-502. DOI
17. Cai Z, Wang J, Lu Z, et al. Ultrafast metal electrodeposition revealed by in situ optical imaging and theoretical modeling towards fast-charging Zn battery chemistry. *Angew Chem Int Ed Engl* 2022;61:e202116560. DOI
18. Naveed A, Rasheed T, Raza B, et al. Addressing thermodynamic instability of Zn anode: classical and recent advancements. *Energy Stor Mater* 2022;44:206-30. DOI
19. Arlt T, Schröder D, Krewer U, Manke I. *In operando* monitoring of the state of charge and species distribution in zinc air batteries using X-ray tomography and model-based simulations. *Phys Chem Chem Phys* 2014;16:22273-80. DOI
20. Fan X, Yang Z, Xie X, Long W, Wang R, Hou Z. The electrochemical behaviors of Zn-Al-La-hydrotalcite in Zn-Ni secondary cells. *J Power Sources* 2013;241:404-9. DOI

21. Chen J, Zhou W, Quan Y, et al. Ionic liquid additive enabling anti-freezing aqueous electrolyte and dendrite-free Zn metal electrode with organic/inorganic hybrid solid electrolyte interphase layer. *Energy Stor Mater* 2022;53:629-37. DOI

22. Hao J, Li X, Zeng X, Li D, Mao J, Guo Z. Deeply understanding the Zn anode behaviour and corresponding improvement strategies in different aqueous Zn-based batteries. *Energy Environ Sci* 2020;13:3917-49. DOI

23. Zhang Y, Zheng X, Wang N, et al. Anode optimization strategies for aqueous zinc-ion batteries. *Chem Sci* 2022;13:14246-63. DOI

24. Liu H, Liu Y, Zhu D. Chemical doping of graphene. *J Mater Chem* 2011;21:3335-45. DOI

25. Zhang J, Zhao Z, Xia Z, Dai L. A metal-free bifunctional electrocatalyst for oxygen reduction and oxygen evolution reactions. *Nat Nanotechnol* 2015;10:444-52. DOI

26. Li L, Tsang YCA, Xiao D, Zhu G, Zhi C, Chen Q. Phase-transition tailored nanoporous zinc metal electrodes for rechargeable alkaline zinc-nickel oxide hydroxide and zinc-air batteries. *Nat Commun* 2022;13:2870. DOI

27. Li G, Mezaal MA, Zhang R, Zhang K, Lei L. Electrochemical performance of MnO_2-based air cathodes for zinc-air batteries. *Fuel Cells* 2016;16:395-400. DOI

28. Li J, Li W, Mi H, et al. Bifunctional oxygen electrocatalysis on ultra-thin Co_9S_8/MnS carbon nanosheets for all-solid-state zinc-air batteries. *J Mater Chem A* 2021;9:22635-42. DOI

29. Sun C, Alonso JA, Bian J. Recent advances in perovskite-type oxides for energy conversion and storage applications. *Adv Energy Mater* 2021;11:2000459. DOI

30. Gao Y, Zhang T, Mao Y, Wang J, Sun C. Highly efficient bifunctional layered triple Co, Fe, Ru hydroxides and oxides composite electrocatalysts for zinc-air batteries. *J Electroanal Chem* 2023;935:117315. DOI

31. Li H, Guo Z, Wang X. Atomic-layer-deposited ultrathin Co_9S_8 on carbon nanotubes: an efficient bifunctional electrocatalyst for oxygen evolution/reduction reactions and rechargeable Zn-air batteries. *J Mater Chem A* 2017;5:21353-61. DOI

32. Niu Y, Gong S, Liu X, et al. Engineering iron-group bimetallic nanotubes as efficient bifunctional oxygen electrocatalysts for flexible Zn-air batteries. *eScience* 2022;2:546-56. DOI

33. Wang Y, Zhang C, Wang X, et al. Engineering carbon-chainmail-shell coated Co_9Se_8 nanoparticles as efficient and durable catalysts in seawater-based Zn-air batteries. *Acta Physico Chimica Sinica* 2024;40:2305004. DOI

34. Han X, He G, He Y, et al. Engineering catalytic active sites on cobalt oxide surface for enhanced oxygen electrocatalysis. *Adv Energy Mater* 2018;8:1702222. DOI

35. Li YW, Zhang WJ, Li J, et al. Fe-MOF-derived efficient ORR/OER bifunctional electrocatalyst for rechargeable zinc-air batteries. *ACS Appl Mater Interfaces* 2020;12:44710-9. DOI

36. Ma J, Li J, Wang R, et al. Hierarchical porous S-doped Fe-N-C electrocatalyst for high-power-density zinc-air battery. *Mater Today Energy* 2021;19:100624. DOI

37. Li G, Mu Y, Huang Z, et al. Poly-active centric Co_3O_4-CeO_2/Co-N-C composites as superior oxygen reduction catalysts for Zn-air batteries. *Sci China Mater* 2021;64:73-84. DOI

38. Chen P, Zhang K, Tang D, et al. Recent progress in electrolytes for Zn-air batteries. *Front Chem* 2020;8:372. DOI

39. Sharma Y, Aziz M, Yusof J, Kordesch K. Triethanolamine as an additive to the anode to improve the rechargeability of alkaline manganese dioxide batteries. *J Power Sources* 2001;94:129-31. DOI

40. Yang H, Cao Y, Ai X, Xiao L. Improved discharge capacity and suppressed surface passivation of zinc anode in dilute alkaline solution using surfactant additives. *J Power Sources* 2004;128:97-101. DOI

41. Zhu Y, Yin J, Zheng X, et al. Concentrated dual-cation electrolyte strategy for aqueous zinc-ion batteries. *Energy Environ Sci* 2021;14:4463-73. DOI

42. Qiu K, Wang F, Liao M, et al. A fumed SiO_2-based composite hydrogel polymer electrolyte for near-neutral zinc-air batteries. *Acta Phys Chim Sin* 2024;40:2304036. DOI

43. Xu M, Ivey DG, Xie Z, Qu W. Electrochemical behavior of Zn/Zn(II) couples in aprotic ionic liquids based on pyrrolidinium and imidazolium cations and bis(trifluoromethanesulfonyl)imide and dicyanamide anions. *Electrochim Acta* 2013;89:756-62. DOI

44. Shinde SS, Jung JY, Wagh NK, et al. Ampere-hour-scale zinc-air pouch cells. *Nat Energy* 2021;6:592-604. DOI

45. Liu Q, Liu R, He C, et al. Advanced polymer-based electrolytes in zinc-air batteries. *eScience* 2022;2:453-66. DOI

46. Xu M, Ivey DG, Xie Z, Qu W. Rechargeable Zn-air batteries: progress in electrolyte development and cell configuration advancement. *J Power Sources* 2015;283:358-71. DOI

47. Wang MY, Huang RB, Xiong JF, Tian JH, Li JF, Tian ZQ. Critical role and recent development of separator in zinc-air batteries. *Acta Phys Chim Sin* 2024;40:2307017. DOI

48. Teng HT, Wang WT, Han XF, Hao X, Yang R, Tian JH. Recent development and perspectives of flexible zinc-air batteries. *Acta Phys Chim Sin* 2023;39:2107017. DOI

49. Lee HJ, Lim JM, Kim HW, et al. Electrospun polyetherimide nanofiber mat-reinforced, permselective polyvinyl alcohol composite separator membranes: a membrane-driven step closer toward rechargeable zinc-air batteries. *J Membr Sci* 2016;499:526-37. DOI

50. Liu Y, Liu S, Xie X, et al. A functionalized separator enables dendrite-free Zn anode via metal-polydopamine coordination chemistry. *InfoMat* 2023;5:e12374. DOI

51. Jana KK, Lue SJ, Huang A, Soesanto JF, Tung KL. Separator membranes for high energy-density batteries. *ChemBioEng Rev* 2018;5:346-71. DOI

52. Boebinger MG, Lewis JA, Sandoval SE, Mcdowell MT. Understanding transformations in battery materials using in situ and operando experiments: progress and outlook. *ACS Energy Lett* 2020;5:335-45. DOI

53. Schröder D, Arlt T, Krewer U, Manke I. Analyzing transport paths in the air electrode of a zinc air battery using X-ray tomography. *Electrochem Commun* 2014;40:88-91. DOI

54. Hack J, Patel D, Bailey JJ, Iacoviello F, Shearing PR, Brett DJL. *In situ* x-ray computed tomography of zinc-air primary cells during discharge: correlating discharge rate to anode morphology. *J Phys Mater* 2022;5:014001. DOI

55. Li G, Mao J, Saqib M, Hao R. Operando optoelectrochemical analysis of single zinc dendrites with a reflective nanopore electrode. *Chem Asian J* 2022;17:e202200824. DOI

56. Mao J, Li G, Saqib M, Xu J, Hao R. Super-resolved dynamics of isolated zinc formation during extremely fast electrochemical deposition/dissolution processes. *Chem Sci* 2022;13:12782-90. DOI

57. Sasaki Y, Yoshida K, Kawasaki T, Kuwabara A, Ukyo Y, Ikuhara Y. *In situ* electron microscopy analysis of electrochemical Zn deposition onto an electrode. *J Power Sources* 2021;481:228831. DOI

58. Li M, Ran L, Knibbe R. Zn electrodeposition by an *in situ* electrochemical liquid phase transmission electron microscope. *J Phys Chem Lett* 2021;12:913-8. DOI

59. Britton MM, Bayley PM, Howlett PC, Davenport AJ, Forsyth M. In situ, real-time visualization of electrochemistry using magnetic resonance imaging. *J Phys Chem Lett* 2013;4:3019-23. DOI

60. Wang T, Kunimoto M, Mori T, et al. Carbonate formation on carbon electrode in rechargeable zinc-air battery revealed by in-situ Raman measurements. *J Power Sources* 2022;533:231237. DOI

61. Santos F, Abad J, Vila M, Castro GR, Urbina A, Fernández Romero AJ. In situ synchrotron x-ray diffraction study of Zn/Bi_2O_3 electrodes prior to and during discharge of Zn-air batteries: influence on ZnO deposition. *Electrochim Acta* 2018;281:133-41. DOI

62. Han X, Zhang T, Chen W, et al. $Mn-N_4$ oxygen reduction electrocatalyst: operando investigation of active sites and high performance in zinc-air battery. *Adv Energy Mater* 2021;11:2002753. DOI

63. Sun Z, Zhang H, Cao L, et al. Understanding synergistic catalysis on Cu-Se dual atom sites via *operando* X-ray absorption spectroscopy in oxygen reduction reaction. *Angew Chem Int Ed Engl* 2023;62:e202217719. DOI

64. Withers PJ, Bouman C, Carmignato S, et al. X-ray computed tomography. *Nat Rev Methods Primers* 2021;1:18. DOI

65. Schröder D, Bender CL, Arlt T, et al. *In operando* x-ray tomography for next-generation batteries: a systematic approach to monitor reaction product distribution and transport processes. *J Phys D Appl Phys* 2016;49:404001. DOI

66. Franke-Lang R, Arlt T, Manke I, Kowal J. X-ray tomography as a powerful method for zinc-air battery research. *J Power Sources* 2017;370:45-51. DOI

67. Chen B, Zhang H, Xuan J, Offer GJ, Wang H. Seeing is believing: in situ/operando optical microscopy for probing electrochemical energy systems. *Adv Mater Technol* 2020;5:2000555. DOI

68. Rukari T, Babita A. Transmission electron microscopy-an overview. *IRJIPS* 2013;1:1-7. Available from: https://www.researchgate.net/publication/332104143_Review_Article_TRANSMISSION_ELECTRON_MICROSCOPY. [Last accessed on 20 Dec 2023]

69. Santhosh Kumar R, Muthu Austeria P, Sagaya Selvam Neethinathan C, et al. Highly mixed high-energy d-orbital states enhance oxygen evolution reactions in spinel catalysts. *Appl Surf Sci* 2023;641:158469. DOI

70. Braidy N, Béchu A, de Souza Terra JC, Patience GS. Experimental methods in chemical engineering: transmission electron microscopy - TEM. *Can J Chem Eng* 2020;98:628-41. DOI

71. Sasaki Y, Yoshida K, Kuwabara A, Ikuhara Y. On-chip electrochemical analysis combined with liquid-phase electron microscopy of zinc deposition/dissolution. *J Electrochem Soc* 2021;168:112511. DOI

72. Mohammadi M, Jerschow A. In situ and operando magnetic resonance imaging of electrochemical cells: a perspective. *J Magn Reson* 2019;308:106600. DOI

73. Hess C. New advances in using Raman spectroscopy for the characterization of catalysts and catalytic reactions. *Chem Soc Rev* 2021;50:3519-64. DOI

74. Campion A, Kambhampati P. Surface-enhanced Raman scattering. *Chem Soc Rev* 1998;27:241-50. DOI

75. Stiles PL, Dieringer JA, Shah NC, Van Duyne RP. Surface-enhanced Raman spectroscopy. *Annu Rev Anal Chem* 2008;1:601-26. DOI

76. Wei X, Wang X, An Q, Han C, Mai L. Operando X-ray diffraction characterization for understanding the intrinsic electrochemical mechanism in rechargeable battery materials. *Small Methods* 2017;1:1700083. DOI

77. Bunaciu AA, Udriştioiu EG, Aboul-Enein HY. X-ray diffraction: instrumentation and applications. *Crit Rev Anal Chem* 2015;45:289-99. DOI

78. Ameh ES. A review of basic crystallography and x-ray diffraction applications. *Int J Adv Manuf Technol* 2019;105:3289-302. DOI

79. Kumar RS, Mannu P, Prabhakaran S, et al. Trimetallic oxide electrocatalyst for enhanced redox activity in zinc-air batteries evaluated by in situ analysis. *Adv Sci* 2023;10:2303525. DOI

80. Wu Z, Kong Pang W, Chen L, Johannessen B, Guo Z. In situ synchrotron X-ray absorption spectroscopy studies of anode materials for rechargeable batteries. *Batteries Supercaps* 2021;4:1547-66. DOI

81. Wang M, Feng Z. Pitfalls in X-ray absorption spectroscopy analysis and interpretation: a practical guide for general users. *Curr Opin Electrochem* 2021;30:100803. DOI

82. Young NA. The application of synchrotron radiation and in particular X-ray absorption spectroscopy to matrix isolated species. *Coord Chem Rev* 2014;277-8:224-74. DOI

83. Kerr BV, King HJ, Garibello CF, et al. Characterization of energy materials with X-ray absorption spectroscopy - advantages, challenges, and opportunities. *Energy Fuels* 2022;36:2369-89. DOI